Acta Mech 197, 1–17 (2008)
DOI 10.1007/s00707-007-0502-4
Printed in The Netherlands

Acta Mechanica

On the dynamic behavior of piezoelectric sensors and actuators embedded in elastic media

X. D. Wang[1], G. L. Huang[2]

[1] Department of Mechanical Engineering, University of Alberta, Edmonton, Alberta, Canada
[2] Department of Systems Engineering, University of Arkansas at Little Rock, Little Rock, AR, USA

Received 15 May 2007; Accepted 22 August 2007; Published online 8 October 2007

Summary. Embedded piezoelectric sensors can be used to monitor the mechanical behaviour of structures for damage detection. This paper provides an analytical study of the dynamic behaviour of piezoelectric sensors embedded in elastic media under high frequency electromechanical loads induced by piezoelectric actuators. A generalized sensor/actuator model taking account of the deformation in both transverse and longitudinal directions of the piezoelectric sensor/actuator is developed. The dynamic load transfer between the sensors/actuators and the host medium is studied using Fourier transform method and solving the resulting integral equations in terms of the interfacial normal and shear stresses. Detailed numerical simulation is conducted to study the relation between the deformation of the sensor and that of the host medium under different loading conditions. The results show the significant effect of the geometry, the material combination and the loading frequency upon the behaviour of the sensor.

1 Introduction

Piezoceramic materials exhibit strong electromechanical coupling and are highly sensitive over a wide range of loading frequencies. Using networks of piezoelectric sensors/actuators in the design of smart structures has attracted significant attention from the industrial and research communities. This new technology is now being used in the position and shape control, the active noise control, the vibration suppression, and the real-time monitoring of structures [1]–[8]. Optimizing the effectiveness and reliability of integrated sensor/actuator systems requires a clear understanding of the sensing/actuating processes and the resulting electromechanical response of the whole structure. When a piezoelectric patch is embbeded in a structure as a sensor, the local mechanical deformation will result in an electric voltage across the thickness of the sensor, which can be recorded by data acquisition systems to evaluate the strain/stress level. Ideally, the piezoelectric sensor should not be intrusive, but in reality the existence of a sensor will disturb the mechanical field to be measured. Since the stiffness of some piezoelectric sensors, piezoceramic ones for example, is comparable to that of typical engineering materials, the disturbance from sensors on the measured signal could be significant.

Correspondence: X. D. Wang, Department of Mechanical Engineering, University of Alberta, Edmonton, Alberta, Canada T6G2G8
e-mail: xiaodong.wang@ualberta.ca

In general cases involving sensors/actuators with finite length and thickness, due to the presence of material discontinuity between the sensors/actuators and the host medium a complicated stress field will be generated when external electromechanical loads are applied. The static behaviour of piezoelectric sensors/actuators has been studied extensively to simulate the sensing/actuating process. A beam with surface-bonded and embedded thin-sheet piezoelectric elements is first analyzed to study the load transfer between piezoelectric elements and the host medium [9], [10]. A refined actuator model based on the plane stress condition is studied to investigate the electromechanical behaviour of a beam with symmetrically surface-bonded actuator patches [11]. Plate and shell models have also been extensively used in modelling the electromechanical behaviour of piezoelectric structures [12]–[16]. The static local stress field near a thin-sheet piezoelectric element attached to an infinite elastic medium is studied to investigate the load transfer between the piezoelectric element and the host medium and the stress concentration [17]. A similar analysis is also conducted to determine the static electromechanical field of a piezoelectric layer bonded to an elastic medium with both interfacial and normal stresses being considered [18], [19].

Piezoelectric sensors/actuators have also been extensively used in vibration sensing and active control [20]–[27] of structures. Typical examples are the use of piezoceramic elements as actuators to excite structures and Polyvinylidene Fluoride (PVDF) films as sensors to monitor their vibration for the identification of natural frequencies and mode shapes. Modal sensors, PVDF films with special shapes, have also been developed to sense specific modal response in vibration [28]. Based on the usage of piezoelectric sensors/actuators, an electromechanical impedance method has been developed and extensively used for damage identification of structures [29]–[31]. It should be mentioned that in most of the studies mentioned above the dynamic interaction between sensors and host structures has been ignored and the received sensor signals have been used directly to evaluate the strain/stress of the structure. The theoretical and experimental study of the vibration of beams with attached piezoelectric sensors [32] indicates that the existence of piezoelectric elements will change the modal shapes and natural frequencies of the beams. To account for the interaction effect between sensors and host structures, correction factors have been introduced to relate the sensor signal and the deformation of the host structure, which has been experimentally validated over a low frequency range of 5–500 Hz [33].

Piezoelectric sensors, because they are quick in response, are also being used for high frequency applications, such as generating and collecting diagnostic elastic waves for damage detection of structures. In these applications, the wavelength is typically comparable or shorter than the length of the sensor. The understanding of the dynamic behaviour of such structures is very limited in comparison with the corresponding low frequency cases. Surface-bonded piezoceramic sensors under high-frequency electric loads have been studied recently using a one-dimensional piezoelectric sensor model [34]. The results show that the dynamic coupling between the sensor and the host structure can significantly change the sensor signal. The dynamic response of embedded piezoelectric sensors, which are considered to be used in advanced structures/materials such as layered media or composites, has not been properly studied. The behaviour of embedded sensors is different from that of the surface ones since for the embedded sensors not only the longitudinal strain, but also the transverse deformation of it will play an important role in the sensing process, especially when the loading frequency is high.

It is therefore the objective of the current paper to provide a comprehensive theoretical study of the dynamic behaviour of embedded piezoelectric sensors. Attention will be focussed on the load transfer between piezoelectric sensors and the host medium, and the electromechanical response of the sensors. A generalized one-dimensional electromechanical model, which includes the deformation in both transverse and longitudinal directions, is used to simulate the behaviour of the sensor. Numerical simulation is conducted to evaluate the effect of the geometry, material

mismatch, and the loading frequency on the resulting strain in the sensor, which represents the strain level in the the host medium to be determined.

2 Formulation of the problem

Consider the two-dimensional plane problem of parallel thin-sheet piezoceramic elements, which act as either sensors or actuators, embedded in a homogeneous and isotropic elastic insulator, as illustrated in Fig. 1. The size of the sensors/actuators is assumed to be significantly smaller than that of the host structure. Therefore, the host structure is modelled as an infinite medium. It is assumed that the poling direction of each piezoceramic sensor/actuator is along its thickness. The half length and the thickness of sensor/actuator A_n are denoted a_n and h_n, respectively, and the centre of it is located at (y_n^0, z_n^0) in the global coordinate (y, z). A local coordinate system (y_n, z_n) is also used to describe sensor/actuator A_n with the origin being at its centre. When the host medium is deformed, an electric voltage will be generated across the upper and lower surfaces of a sensor. In the current integrated sensor/acuator system, the deformation of the host medium is induced by applying a voltage between the upper and the lower surfaces of actuator A_n, which generates an electric field of frequency ω along the thickness direction of the actuator $E_z^n = (V_n^- - V_n^+)/h_n$, with V_n^+ and V_n^- being the electric potentials at the upper and the lower electrodes, respectively. Because of the piezoelectric property of the actuator, elastic waves will be induced in the host medium.

The plane strain deformation will be assumed in this paper. Compared to the small thickness of the piezoelectric sensor (typically 0.15 mm to 0.5 mm), the width of the piezoelectric thin-sheets in the direction perpendicular to the $y{-}z$ plane is significantly larger. For the current embedded piezoelectric thin-sheet sensor, high stress concentration exists near the end of it. The deformation corresponding to the high stresses near the end of the sensor will, however, be restrained by the surrounding materials of both the sensor and the host medium. Limiting the deformation of the sensor in the direction of the width will form a plane strain condition. It should also be mentioned that no viscous effect is included in the current analysis and only non-dispersive wave propagation is considered. For the steady state response of the system discussed in this paper, the time factor $\exp(-i\omega t)$, which applies to all the field variables, will be suppressed. Existing studies indicate that the interaction between piezoelectric elements under dynamic loads is usually very weak unless they are in close proximity. In the current study, attention will be focussed on the cases where piezoelectric elements are relatively far away and the interaction between the actuator and the sensor will be ignored.

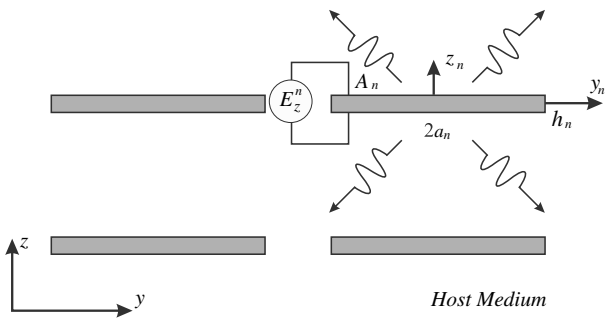

Fig. 1. Embedded sensors/actuators in an elastic medium

2.1 Modelling of the sensor/actuator

The sensor and the actuator will behave differently in an integrated system. For the actuator, a high frequency electric field E_z across its thickness is applied, which results in elastic waves in the host medium with the typical wavelength being comparable to the length of the actuator. For the sensor, the resulting elastic wave in the host medium will act as the incident wave. In this case, the inertia effect of the sensor/actuator must be considered.

For an embedded thin-sheet sensor/actuator, its thickness is usually small in comparison with the length. It can then be assumed that the stress and strain components σ_y^s, σ_z^s, ε_y^s, ε_z^s and displacement u_y^s are uniformly distributed across the thickness. The sensor/actuator can be regarded as a one-dimensional electromechanical element subjected to τ and σ_z, as shown in Fig. 2, in which τ and σ_z represent the interfacial shear and normal stresses between the sensor and the host medium. According to these assumptions the equation of motion of the sensor/actuator in the axial direction can be expressed as

$$\frac{d\sigma_y^s}{dy} + \tau(y)/h + \rho_s \omega^2 u_y^s = 0, \tag{1}$$

where ρ_s is the mass density of the sensor/actuator. The transverse deformation of the sensor/actuator is given by

$$\varepsilon_z^s(y) = \frac{u_z^{s+} - u_z^{s-}}{h}, \tag{2}$$

with u_z^{s+}, u_z^{s-} being the displacements at the upper and lower surfaces of the sensor/actuator and h being the thickness of the sensor/actuator. The coupled electromechanical behaviour of the sensor/actuator can be described in terms of the following constitutive equations:

$$\sigma_y^s = c_{11}\varepsilon_y^s + c_{31}\varepsilon_z^s - e_{31}E_z, \tag{3}$$

$$\sigma_z^s = c_{31}\varepsilon_y^s + c_{33}\varepsilon_z^s - e_{33}E_z, \tag{4}$$

$$D_z^s = e_{13}\varepsilon_y^s + e_{33}\varepsilon_z^s + \lambda_{33}E_z, \tag{5}$$

where c_{11}, c_{31}, c_{33} are the elastic constants, e_{31} and e_{33} are the piezoelectric constants, λ_{33} is the dielectric constant, and ε_y^s is the axial strain of the sensor/actuator given by

$$\varepsilon_y^s = \frac{du_y^s}{dy}. \tag{6}$$

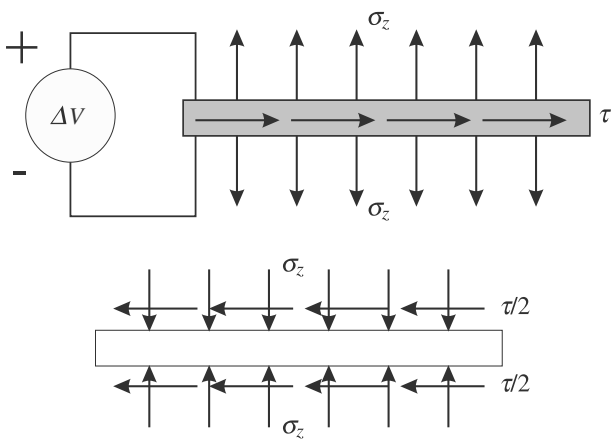

Fig. 2. The sensor model and the interfacial forces

It is assumed that the sensor will operate in the open-loop mode [13], [35]. Since no external charge is supplied, the electric displacement across the thickness of the sensor will be zero, i.e.,

$$D_z = 0. \tag{7}$$

Using this sensor/actuator model, the axial strain of the actuator/sensor can be determined in terms of τ and $(u_z^{a+} - u_z^{a-})$ by solving Eq. (1) as

$$\begin{aligned}\varepsilon_y^s(y) = \varepsilon_E(y) - \int_{-a}^{y} \cos k_s(\xi - y)\frac{p(\xi)}{h\bar{c}_{11}}d\xi \\ + \frac{\sin k_s(a+y)}{h\bar{c}_{11}\sin 2k_s a}\int_{-a}^{s} \cos k_s(\xi - a)p(\xi)d\xi,\end{aligned} \tag{8}$$

where

$$\varepsilon_E(y) = \begin{cases} \frac{e_{31}E_z}{c_{11}}\frac{\cos k_s y}{\cos k_s a} & \text{for actuator} \\ 0 & \text{for sensor} \end{cases}, \tag{9}$$

and $p(y)$ is given by

$$p(y) = \tau(y) + h\bar{c}_{31}\frac{d}{dy}(u_z^{a+} - u_z^{a-}) \tag{10}$$

and

$$\begin{aligned} k_s = \omega/c_s, c_s = \sqrt{\bar{c}_{11}/\rho_s}, \bar{c}_{11} = \begin{cases} c_{11} & \text{for actuator} \\ c_{11} + \frac{e_{31}^2}{\varepsilon_{33}} & \text{for sensor} \end{cases}, \\ \bar{c}_{31} = \begin{cases} c_{31} & \text{for actuator} \\ c_{31} + \frac{e_{31}e_{33}}{\varepsilon_{33}} & \text{for sensor} \end{cases}, \end{aligned} \tag{11}$$

with k_s and c_s being the wave number and the axial wave speed of the actuator/sensor, respectively.

The transverse stress of the sensor/actuator, $\sigma_z^s(y)$, can be expressed, using Eqs. (4) and (8), as

$$\begin{aligned}\sigma_z^s(y) = \sigma_E(y) + \frac{\bar{c}_{31}\sin k_s(a+y)}{h\bar{c}_{11}\sin 2k_s a}\int_{-a}^{s} p(\xi)\cos k_s(\xi - a)d\xi \\ - \frac{\bar{c}_{31}}{h\bar{c}_{11}}\int_{-a}^{y} p(\xi)\cos k_s(\xi - y)d\xi + \frac{\bar{c}_{33}}{h}(u_z^{a+} - u_z^{a-}),\end{aligned} \tag{12}$$

where

$$\begin{aligned} \sigma_E(y) = \begin{cases} c_{31}\varepsilon_E(y) - e_{33}E_z & \text{for actuator} \\ 0 & \text{for sensor} \end{cases}, \\ \bar{c}_{33} = \begin{cases} c_{33} & \text{for actuator} \\ c_{33} + \frac{e_{33}^2}{\varepsilon_{33}} & \text{for sensor.} \end{cases} \end{aligned} \tag{13}$$

For a sensor, the electric displacement can be obtained from the constitutive relation as

$$D_z = e_s\varepsilon_y + d_s\sigma_z + \lambda_s E_z, \tag{14}$$

where e_s, d_s and λ_s are effective material constants given in Appendix A. Under the open-loop mode no external charge is supplied and the piezoelectric charge collected on the two electrodes will

generate an electric field. Using Eqs. (7) and (14), the voltage along the sensor can be determined in terms of the strains as

$$V_z = \frac{h}{\lambda_s}(e_s\varepsilon_y + d_s\sigma_z). \tag{15}$$

Since the voltage is linearly dependent on ε_y and σ_z, in the following discussion attention will be focussed on the strain and stress in the sensor.

2.2 Dynamic behaviour of the integrated electromechanical system

For the host medium with an embedded sensor/actuator, the total mechanical field (u^T) generally consists of two parts, the known incident wave (u^I) and the outgoing wave (u) caused by the sensor/actuator. Since the displacement and traction will be continuous at the upper and lower interfaces of the sensor/actuator, the displacement field can be expressed as

$$u^T = u^I + u. \tag{16}$$

Based on the current sensor/actuator model, the displacement in y-direction is continuous, such that

$$u_y(y, 0^+) = u_y(y, 0^-). \tag{17}$$

Because the sensor/actuator will be deformed in the thickness direction, the host medium will have a crack-like opening $u_z(y,\ 0^+) - u_z(y,\ 0^-)$ at the site of the sensor/actuator. In addition, the sensor/actuator will cause discontinuity of the shear stress across its thickness in the host medium. The interfacial shear stress difference between the upper and the lower surfaces of the 'crack' forms a shear force τ for the sensor/actuator, which has been discussed in the previous Subsection, i.e.,

$$\sigma_{yz}(y, 0^+) - \sigma_{yz}(y, 0^-) = \tau, \quad |y| < a. \tag{18}$$

In the following discussion, the opening deformation of the 'crack' will be represented by the rate of change of it with respect to y, which is denoted by ϕ, i.e.

$$\phi(y) = \frac{\partial}{\partial y}[u_z(y, 0^+) - u_z(y, 0^-)], \quad |y| < a. \tag{19}$$

The opening deformation ϕ and the shear stress τ acting on the 'crack' surfaces will result in an outgoing elastic wave, which can be determined by solving an elastodynamic problem [36] under the conditions given by (17)–(19). The general solution can be expressed as

$$\varepsilon_y(y, 0)|_{\text{matrix}} = -\frac{1}{2\pi\mu}\left[\int_{-a}^{a} \tau(\xi)n_1(y-\xi)d\xi + \mu\int_{-a}^{a} \phi(\xi)n_2(y-\xi)d\xi\right], \tag{20}$$

$$\sigma_z(y, 0)|_{\text{matrix}} = -\frac{1}{2\pi}\left[\int_{-a}^{a} \tau(\xi)n_2(y-\xi)d\xi + \mu\int_{-a}^{a} \phi(\xi)n_3(y-\xi)d\xi\right], \tag{21}$$

where μ is the shear modulus of the host medium and

$$n_1(y-\xi) = \frac{1}{k^2}\int_0^{\infty} \frac{s(s^2 - \alpha\beta)}{\alpha}\sin s(\xi - y)ds, \tag{22}$$

$$n_2(y-\xi)=\frac{1}{k^2}\int_0^\infty \frac{s(-\gamma+2\alpha\beta)}{\alpha}\sin s(\xi-y)ds, \tag{23}$$

$$n_3(y-\xi)=\frac{1}{k^2}\int_0^\infty \frac{(\gamma^2-4s^2\alpha\beta)}{s\alpha}\sin s(\xi-y)ds \tag{24}$$

with $\gamma = s^2 + \beta^2$ and

$$\alpha=\begin{cases}\sqrt{s^2-K^2} & |s|>K\\ -i\sqrt{K^2-s^2} & |s|<K\end{cases}\qquad \beta=\begin{cases}\sqrt{s^2-k^2} & |s|>k\\ -i\sqrt{k^2-s^2} & |s|<k\end{cases}, \tag{25}$$

$$K=\omega/c_L, k=\omega/c_T. \tag{26}$$

c_L and c_T are the longitudinal and transverse shear wave speeds of the elastic medium, respectively.

The 'crack' opening ϕ and the shear stress τ satisfy the following continuity condition between the sensor/actuator and the host medium, as given by (16):

$$\begin{aligned}&\varepsilon_y^s(y)=\varepsilon_y(y,0)+\varepsilon_y^I(y,0),\\ &\sigma_z^s(y)=\sigma_z(y,0)+\sigma_z^I(y,0),\quad |y|<a,\end{aligned} \tag{27}$$

where $\varepsilon_y(y, 0)$, $\sigma_z(y, 0)$ are caused by the outgoing wave given by (20) and (21), and the terms with superscripts $'a'$ and $'I'$ represent the sensor/actuator and the known incident field, respectively. It should be mentioned that for the case of an actuator the incident wave does not exist.

By substituting Eqs. (8), (12), (20) and (21) into Eq. (27), the following integral equations can be obtained:

$$\begin{aligned}&-\frac{1}{2\pi\mu}\int_{-a}^{a}\Big[\tau(\xi)n_1(y-\xi)+\mu\phi(\xi)n_2(y-\xi)\Big]d\xi\\ &\quad-\frac{\sin k_s(a+y)}{h\bar{c}_{11}\sin 2k_sa}\int_{-a}^{s}\Big[\tau(\xi)+\bar{c}_{31}\phi(\xi)\Big]\cos k_s(\xi-a)d\xi\\ &\quad+\frac{1}{h\bar{c}_{11}}\int_{-a}^{y}\Big[\tau(\xi)+\bar{c}_{31}\phi(\xi)\Big]\cos k_s(\xi-y)d\xi=\varepsilon_E(y)-\varepsilon_y^I(y,0),\quad |y|<a,\end{aligned} \tag{28}$$

$$\begin{aligned}&-\frac{1}{2\pi}\int_{-a}^{a}\Big[\tau(\xi)n_2(y-\xi)+\mu\phi(\xi)n_3(y-\xi)\Big]d\xi-\frac{\bar{c}_{33}}{h}\int_{-a}^{y}\phi(\xi)d\xi\\ &\quad+\frac{\bar{c}_{31}}{h\bar{c}_{11}}\int_{-a}^{y}\Big[\tau(\xi)+\bar{c}_{31}\phi(\xi)\Big]\cos k_s(\xi-y)d\xi=\sigma_E(y)-\sigma_z^I(y,0),\quad |y|<a.\end{aligned} \tag{29}$$

Equations (28) and (29) involve a square-root singularity for both τ and ϕ at the ends of the sensor/actuator. The general solutions of τ and ϕ can then be expressed in terms of Chebyshev polynomials as

$$\begin{aligned}&\tau(y)=\sum_{j=0}^{\infty}A_jT_j(y/a)/\sqrt{1-y^2/a^2},\\ &\phi(y)=\sum_{j=0}^{\infty}B_jT_j(y/a)/\sqrt{1-y^2/a^2},\end{aligned} \tag{30}$$

with T_j being Chebyshev polynomials of the first kind and A_j and B_j being unknown constants to be determined. If the expansions in (30) are truncated to the Nth term and Eqs. (28) and (29) are satisfied at the following collocation points along the sensor/actuator:

$$y^l = a\cos\left[\frac{l-1}{N-1}\pi\right], \quad l = 1,2,\cdots,N, \tag{31}$$

$2N$ linear algebraic equations in terms of $\{c\} = \{A_0, A_1, \ldots, A_{N-1}, B_1, B_2, \ldots, B_{N-1}\}^T$ can be obtained. These equations can be represented as

$$[Q]\{c\} = \{F\}, \tag{32}$$

where $[Q]$ is a known matrix given in Appendix B, and the general loading $\{F\}$ is given by

$$\begin{aligned} F_l &= \varepsilon_E(y^l) - \varepsilon^I(y^l, 0) \quad l = 1,2,\ldots,N \\ F_l &= \sigma_E(y^l) - \sigma^I(y^l, 0) \quad l = N+1, N+2, \ldots, 2N. \end{aligned} \tag{33}$$

Based on the solution of τ and ϕ, the dynamic stress and strain field in both the sensor/actuator and the matrix can be determined.

3 Results and discussion

This Section will be devoted to the discussion of the static and dynamic behaviour of embedded piezoelectric sensors. The incident wave is applied through a piezoelectric actuator subjected to a harmonic electric load (voltage). Attention will be focussed on the effects of material property, the geometry and loading frequency upon the the response of the sensors.

The incident field is induced by a piezoelectric actuator parallel to the sensor, which is subjected to an electric voltage of frequency ω across its thickness. Based on the solution given in Subsect. 2.2, the strain and stress components ε^I and σ^I in the matrix induced by the actuator can be determined as

$$\begin{aligned} \varepsilon_y^I(y^*, z^*) = \frac{-1}{2\pi k^2}\Bigg[& \int_{-a}^{a} \tau^{(a)}(u) \int_{-\infty}^{\infty} \frac{s^3}{\alpha} e^{-\alpha|z^*|} - s\beta e^{-\beta|z^*|} \sin s(u - y^*) ds du \\ & + \mu \int_{-a}^{a} \phi^{(a)}(u) \int_{-\infty}^{\infty} -\frac{s\gamma}{\alpha} e^{-\alpha|z^*|} + 2s\beta e^{-\beta|z^*|} \sin s(u - y^*) ds du \Bigg], \end{aligned} \tag{34}$$

$$\begin{aligned} \sigma_y^I(y^*, z^*) = \frac{-1}{\pi k^2}\Bigg[& \int_{-a}^{a} \tau^{(a)}(u) \int_{-\infty}^{\infty} -\frac{s\gamma}{2\alpha} e^{-\alpha|z^*|} + s\beta e^{-\beta|z^*|} \sin s(u - y^*) ds du \\ & + \mu \int_{-a}^{a} \phi^{(a)}(u) \int_{-\infty}^{\infty} \frac{\gamma^2}{2\alpha s} e^{-\alpha|z^*|} - 2s\beta e^{-\beta|z^*|} \sin s(u - y^*) ds du \Bigg] \end{aligned} \tag{35}$$

with $\tau^{(a)}$, $\phi^{(a)}$ being given by the solution of Eq. (30) of the actuator. In these equations, $y^* = y - y_a^0$, $z^* = z - z_a^0$ with y and z being the coordinates measured from the centre of the sensor, and y_a^0 and z_a^0 being the position of the centre of the actuator.

At the position of the sensor, the following strain and stress components of the incident wave can be obtained:

$$\varepsilon^I(y,0) = \varepsilon^I_y(y - y^0_a, -z^0_a), \tag{36}$$

$$\sigma^I(y,0) = \sigma^I_z(y - y^0_a, -z^0_a), \tag{37}$$

which are used in (32) and (33) for the solution of the sensor problem.

3.1 Static behaviour of the sensor

Consider first the quasi-static behaviour of an embedded sensor when the loading frequency is very low such that the typical wavelength of the elastic wave in the host medium is much longer than the length of the sensor. The material constants of the sensor and the host medium are assumed to be *Sensor (PZT)* [37]

$$c^{(a)}_{11} = 13.9 \times 10^{10}(Pa), \quad c^{(a)}_{12} = 6.78 \times 10^{10}(Pa), \quad c^{(a)}_{13} = 7.43 \times 10^{10}(Pa),$$
$$c^{(a)}_{33} = 11.5 \times 10^{10}(Pa), \quad c^{(a)}_{44} = 2.56 \times 10^{10}(Pa),$$
$$e^{(a)}_{31} = -5.2(C/m^2), \quad e^{(a)}_{33} = 15.1(C/m^2), \quad e^{(a)}_{15} = 12.7(C/m^2),$$
$$\varepsilon^{(a)}_{11} = 6.45 \times 10^{-9}(C/Vm), \quad \varepsilon^{(a)}_{33} = 5.62 \times 10^{-9}(C/Vm)$$

Host medium

$$E = 2.74 \times 10^{10}(Pa), \quad v = 0.3.$$

The local strain ε^s_y and transverse stress σ^s_z along the sensor can be obtained from Eqs. (8) and (12). The following strain and stress ratios at the position of the sensor between the sensor response and the incident field are introduced and used to evaluate the property of the sensor in predicting the mechanical field in the host medium:

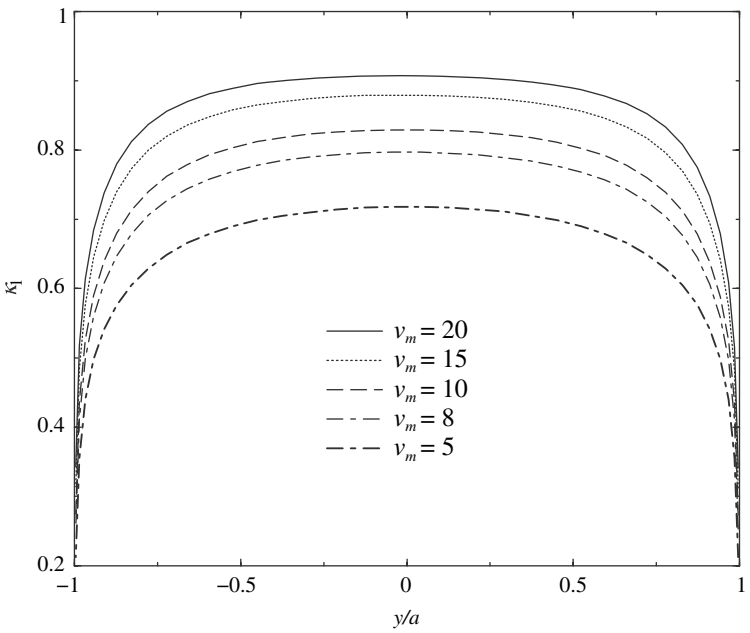

Fig. 3. The static strain ratio for a PZT sensor

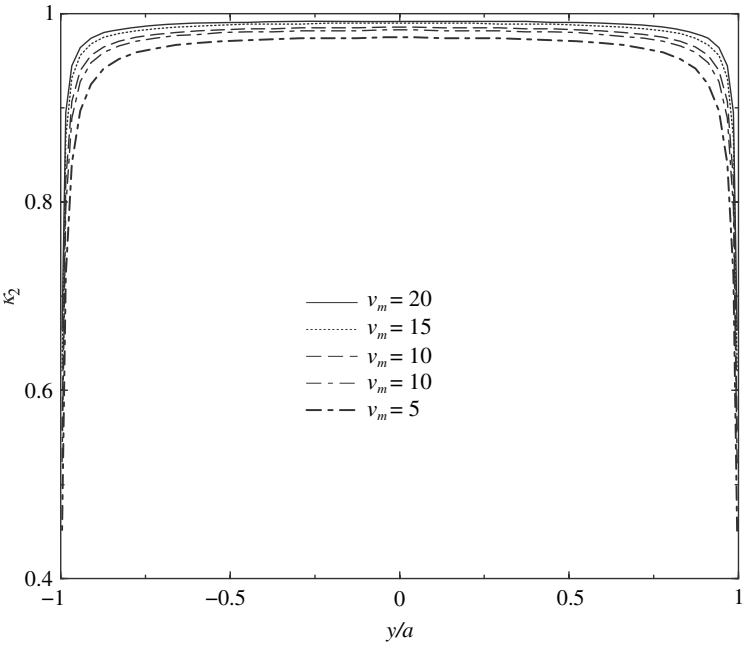

Fig. 4. The static stress ratio for a PZT sensor

$$\kappa_1(y) = \frac{\varepsilon_y^s(y)}{\varepsilon_y^I(y)}, \quad \kappa_2(y) = \frac{\sigma_z^s(y)}{\sigma_z^I(y)}. \tag{38}$$

Ideally, if the sensor does not disturb the incident field these values should be one. The change of these two parameters represents the intrusive effect of the sensor on the original incident field.

Figures 3 and 4 show the effect of the length-to-thickness ratio of the sensor $v_s = a/h$ upon $\kappa_1 = \frac{\varepsilon_y^s(y)}{\varepsilon_y^I(y)}$ and $\kappa_2 = \frac{\sigma_z^s(y)}{\sigma_z^I(y)}$ for the case where the actuator is centrally aligned with the sensor with a distance $e_z = 10a$ and the length-to-thickness ratio of the actuator is $v_a = 20$. It is assumed that the length of the sensor $2a$ is a constant for all the cases considered and the thickness of the sensor changes with v_s. The ratio κ_1, which represents the level of the strain transferred from the host medium to the sensor, decreases dramatically with increasing thickness of the sensor. However, the effect of the thickness of the sensor on the transverse stress transfer, represented by κ_2, is relatively insignificant in comparison with the change in κ_1.

The corresponding results for the case of a PVDF sensor are shown in Figs. 5 and 6. The property of the PVDF sensor is *Sensor (PVDF)*

$$c_{11}^{(a)} = 2.5 \times 10^9(Pa), \quad c_{12}^{(a)} = 0.75 \times 10^9(Pa), \quad c_{13}^{(a)} = 0.75 \times 10^9(Pa),$$
$$c_{33}^{(a)} = 0.9 \times 10^9(Pa), \quad c_{44}^{(a)} = 0.25 \times 10^9(Pa),$$
$$e_{31}^{(a)} = 4.6 \times 10^{-3}(C/m^2), \quad e_{33}^{(a)} = -3.4 \times 10^{-3}(C/m^2), \quad e_{15}^{(a)} = -1.7 \times 10^{-3}(C/m^2),$$
$$\varepsilon_{11}^{(a)} = 0.106 \times 10^{-9}(C/Vm), \quad \varepsilon_{33}^{(a)} = 0.106 \times 10^{-9}(C/Vm).$$

In comparison with the result for PZT sensors, the PVDF sensor shows much higher strain transfer ratio for a given length-to-thickness ratio. For both strain transfer ratio κ_1 and stress transfer ratio κ_2, the thickness shows a significant effect, which is different from the case of PZT sensors.

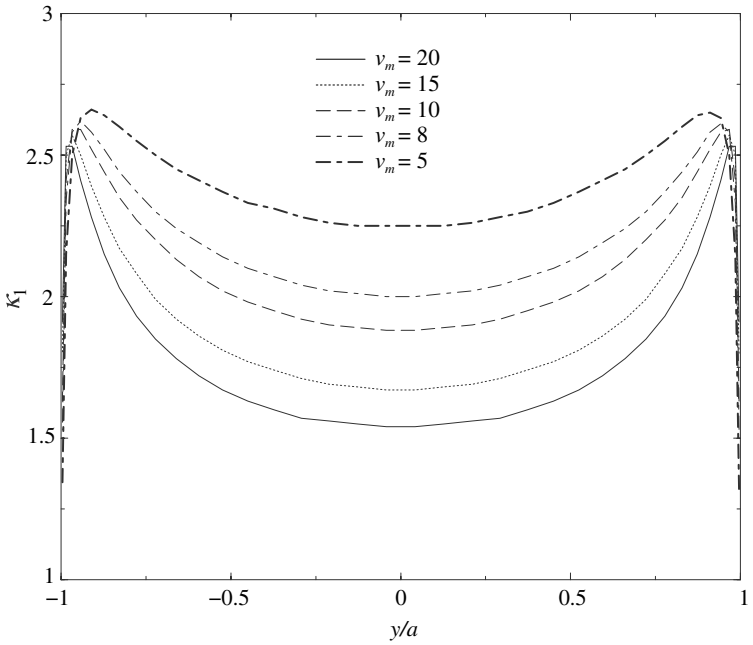

Fig. 5. The static strain ratio for a PVDF sensor

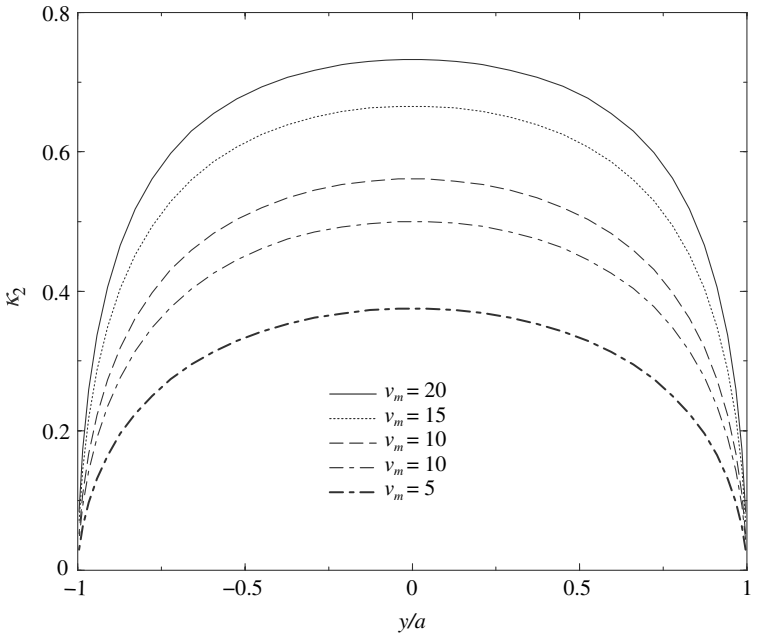

Fig. 6. The static stress ratio for a PVDF sensor

Figures 7 and 8 show the distribution of κ_1 and κ_2 along the sensor for the case where $v_s = 20, \frac{c_{12}}{c_{11}} = \frac{c_{13}}{c_{11}} = 0.5$, for different material combinations $q = \frac{\pi E}{2c_{11}}$. A higher strain transfer ratio κ_1 is observed for higher material combination q, corresponding to a softer sensor. The stress transfer ratio κ_2, however, decreases with increasing q.

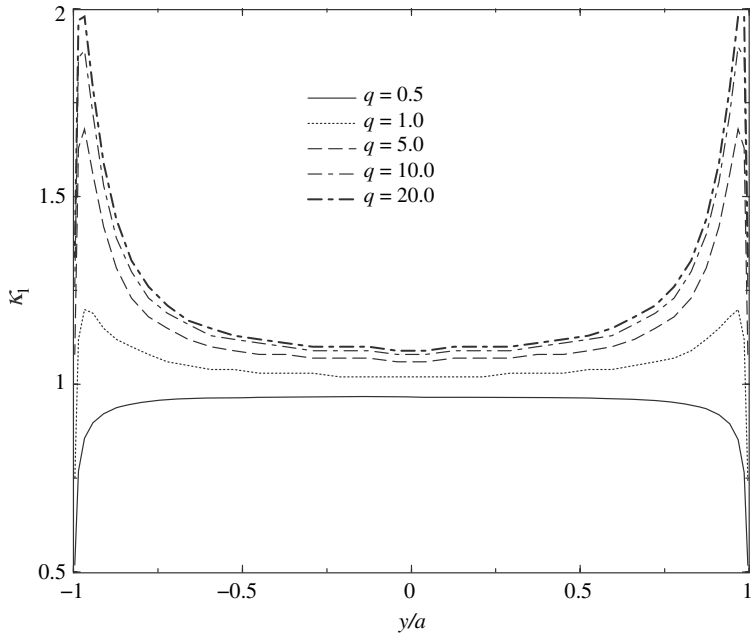

Fig. 7. The static strain ratio for different material combinations

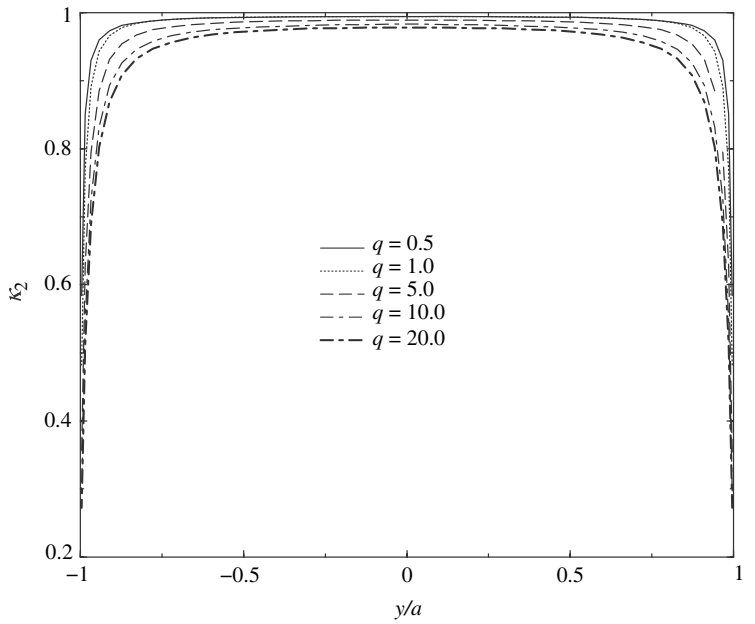

Fig. 8. The static stress ratio for different material combinations

3.2 Dynamic behaviour of the sensor

Figures 9 and 10 show the amplitudes of the dynamic strain and stress transfer ratio κ_1 and κ_2 between a PZT sensor and the host medium for the case where $v_s = 20$, $q = 0.3$, and $\rho_s/\rho_H = 1$, with ρ_s and ρ_H being the mass density of the sensor and the host medium, respectively. In the central part

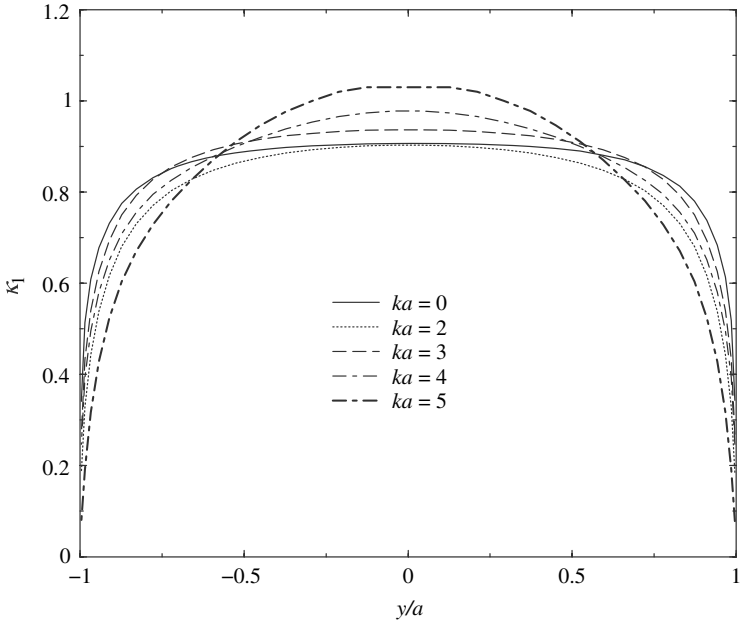

Fig. 9. The dynamic strain ratio for a PZT sensor

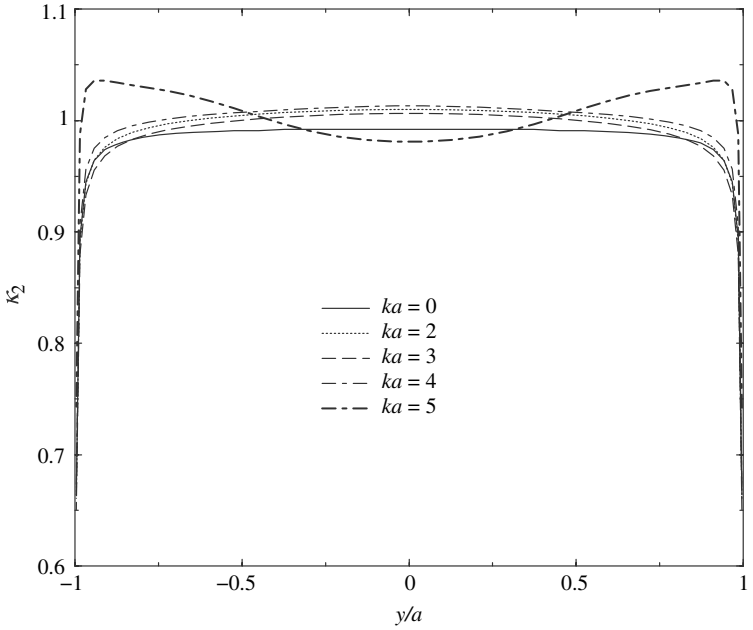

Fig. 10. The dynamic stress ratio for a PZT sensor

of the sensor the strain transfer ratio κ_1 increases with increasing loading frequency (ka). But the effect of the loading frequency upon the stress transfer ratio κ_2, oscillating around $\kappa_2 = 1$ with the change of ka, is not as significant as that on the strain transfer ratio.

The corresponding amplitudes of the dynamic strain and stress transfer ratio κ_1 and κ_2 along a PVDF sensor are shown in Figs. 11 and 12 where $v_s = 20$, $q = 26.5$, and $\rho_s/\rho_H = 0.3$. In this case the

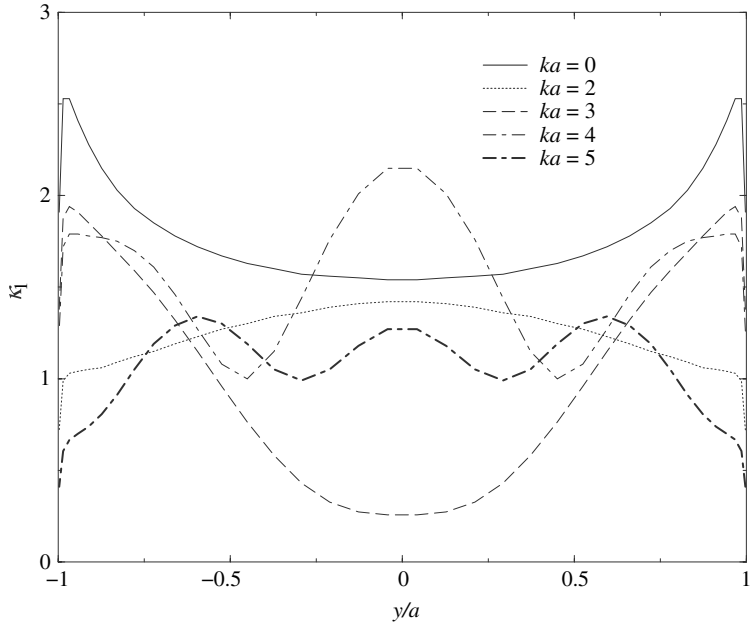

Fig. 11. The dynamic strain ratio for a PVDF sensor

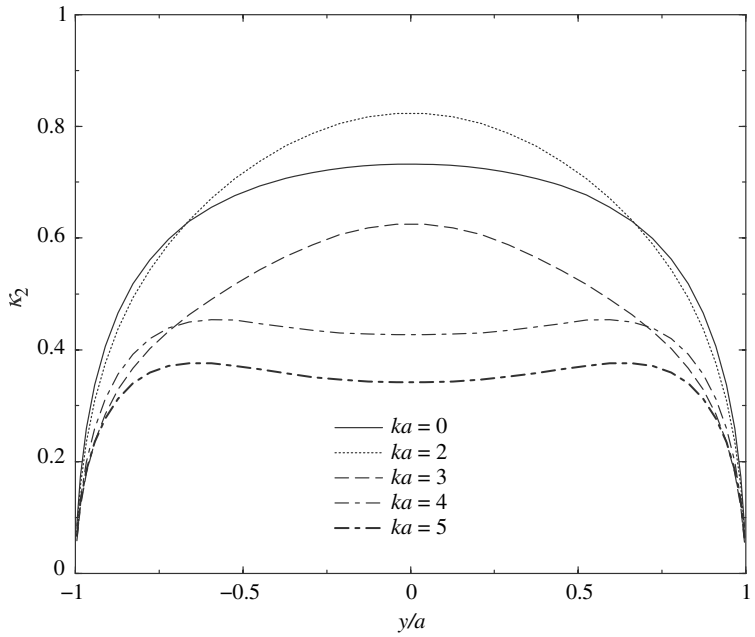

Fig. 12. The dynamic stress ratio for a PVDF sensor

effect of the loading frequency ($k\alpha$) upon both the strain and stress transfer ratios is significant. κ_1 and κ_2 decrease with increasing loading frequency $k\alpha$.

The results discussed indicate that the relation between the sensor response and the incident wave is complicated in most of the cases considered. It should also be mentioned that different from the

case of the surface bonded-sensor [37], both longitudinal strain and transverse stress of an embedded sensor will contribute to the electric voltage output of the sensor.

4 Concluding remarks

An analytical solution is provided to study the static and dynamic electromechanical behaviour of piezoelectric sensors embedded in the elastic medium under plane mechanical and electrical loads. The analysis is based on the use of a generalized one dimensional sensor/actuator model. The effect of the different sensor parameters and the loading frequency upon the behaviour of the sensor is studied. The results show the necessity to account for the interaction between the sensor and the host medium due to the material mismatch, especially for relatively high loading frequencies. Further theoretical and experimental studies are necessary for determining the dynamic strain in the host medium using embedded piezoelectric sensors under high loading frequency.

Appendix A

Effective material constants

The electromechanical behaviour of piezoelectric materials can be described by

$$\{\sigma\} = [c]\{\varepsilon\} - [e]\{E\}, \quad \{D\} = [e]\{\varepsilon\} + [\lambda]\{E\}.$$

In these equations, $\{\sigma\}$ and $\{\varepsilon\}$ are the stresses and the strains, while $\{D\}$, $\{E\}$ represent the electric displacement and the electric field intensity, respectively. $[c]$ is a matrix containing the elastic stiffness parameters, $[e]$ represents the piezoelectric constants and $[\lambda]$ represents the dielectric constants.

For a sensor under open-loop mode (D_z = 0), Eqs. (3), (4) and (5) result in

$$E_z = -(e_{13}\varepsilon_y + e_{33}\varepsilon_z)/\lambda_{33},$$
$$\sigma_z = c^*_{13}\varepsilon_y + c^*_{33}\varepsilon_z,$$
$$\varepsilon_z = (\sigma_z - c^*_{13}\varepsilon_y)/c^*_{33}.$$

Equation (5) can then be expressed in terms of ε_y and σ_z and E_z as

$$D_z = e_s\varepsilon_y + d_s\sigma_z + \lambda_s E_z$$

with the effective material constants of the sensor being given by

$$e_s = e_{13} - \frac{e_{33}c^*_{13}}{c^*_{33}},$$
$$d_s = \frac{e_{33}}{c^*_{33}},$$
$$\lambda_s = \lambda_{33}.$$

Appendix B

Sensor/actuator solution

The matrix $[Q]$ used in Eq. (32) for solving the single sensor/actuator problem is given by

$$
\begin{aligned}
Q_{lj} = & -\pi \sum_{j=1}^{\infty} c_j \frac{\sin\left[j \cos^{-1} \eta^l\right]}{\sin\left[\cos^{-1} \eta^l\right]} \\
& + \pi \sum_{j=1}^{\infty} c_j \int_0^{\infty} P_j^1(\bar{s}, \eta^l) \left(\frac{2\bar{k}^2 \bar{s} \bar{\beta}}{\lambda_0 [(2\bar{s}^2 - \bar{k}^2)^2 - 4\bar{s}^2 \bar{\alpha} \bar{\beta}]} + 1 \right) d\bar{s} \\
& + qv \sum_{j=1}^{\infty} c_j \int_{\cos^{-1} \eta^l}^{\pi} \cos[\overline{k_s}(\cos\theta - \eta^l)] \cos(j\theta) d\theta \\
& - qv \frac{\sin[\bar{k}_s(\eta^l + 1)]}{\sin(2\bar{k}_s)} \sum_{j=1}^{\infty} c_j P_j^2.
\end{aligned}
$$

In the above equations,

$$\eta^l = y^l/a, \quad \bar{K} = Ka, \quad \bar{k} = ka, \quad \overline{k_s} = k_s a, \quad \bar{s} = sa$$

and

$$P_j^1(\bar{s}, \eta^l) = J_j(\bar{s}) \begin{cases} (-1)^n \cos(\bar{s}\eta^l) & j = 2n+1 \\ (-1)^{n+1} \sin(\bar{s}\eta^l) & j = 2n \end{cases}$$

$$P_j^2 = J_j(\bar{s}) \begin{cases} (-1)^n \sin(\bar{k}_s) & j = 2n+1 \\ (-1)^n \cos(\bar{k}_s) & j = 2n \end{cases}$$

with J_j (j = $1, 2 \ldots$) being the Bessel functions of the first kind.

$\bar{\alpha}, \bar{\beta}$ can be obtained from α, β directly, which are defined in Eq. (25), with s, K, k being replaced by $\bar{s}, \bar{K}, \bar{k}$, respectively.

Acknowledgements

This work was supported by the Natural Sciences and Engineering Research Council of Canada. G. L. Huang acknowledges the partial financial support for this research by the National Science Foundation Grant No. EPS-0701890.

References

[1] Gandhi, M. V., Thompson, B. S.: Smart materials and structures. London: Chapman Hall 1992.
[2] Chee, C., Tong, L., Steven, G. P.: A review on the modeling of piezoelectric sensors and actuators incorporated in intelligent structures. J. Intell. Mater. Syst. Struct. **9**, 3–19 (1998).
[3] Boller, C.: Next generation structural health monitoring and its integration into aircraft design. Int. J. Sys. Sci. **31**, 1333–1349 (2000).
[4] Bar-Cohen, Y.: Emerging NDE technologies and challenges at the beginning of the 3rd millennium – Part I. Mater. Eval. **58**, 17–30 (2000).
[5] Banks, H. T., Smith, R. C., Wang, Y.: Smart material structures: modelling, estimation and control. Paris: Masson/Wiley 1996.
[6] Dalton, R. P., Cawley, P., Lowe, M.: The potential of guided waves for monitoring large areas of metallic aircraft fuselage structure. J. Nondestr. Eval. **20**, 29–46 (2001).
[7] Giurgiutiu, V., Zagrai, A., Bao, J. J.: Piezoelectric wafer embedded active sensors for aging aircraft structural health monitoring. Struct. Health Monit. **1**, 41–61 (2002).
[8] Fukunaga, H., Hu, N., Chang, F. K.: Structural damage identification using piezoelectric sensors. Int. J. Solids Struct. **39**, 393–418 (2001).

[9] Crawley, E. F., de Luis, J.: Use of piezoelectric actuators as elements of intelligent structures. AIAA J. **25**, 1373–1385 (1987).
[10] Crawley, E. F., Anderson, E. H.: Detailed models of piezoelectric actuation of beams. J. Intell. Mat. Syst. Struct. **1**, 4–25 (1990).
[11] Lin, M. W., Rogers, C. A.: Actuation response of a beam structure with induced strain actuators. Adap. Struct. Mat. Syst. **35**, 129–139 (1993).
[12] Dimitriadis, E. K., Fuller, C. R., Rogers, C. A.: Piezoelectric actuators for distributed vibration excitation of thin plates. ASME J. Vibr. Acoust. **113**, 100–107 (1991).
[13] Tzou, H. S., Tseng, C. I.: Distributed vibration control and identification of coupled elastic/piezoelectric systems. Mech. Syst. Signal Proces. **5**, 215–231 (1991).
[14] Mitchell, J. A., Reddy, J. N.: A study of embedded piezoelectric layers in composite cylinders. ASME J. Appl. Mech. **62**, 166–173 (1995).
[15] Banks, H. T., Smith, R. C.: The modelling of piezoceramic patch interactions with shells, plates, and beams. Q. Appl. Math. **LIII**, 353–381 (1995).
[16] Han, J. H., Lee, I.: Analysis of composite plates with piezoelectric actuators for vibration control using layerwise displacement theory. Composites Part B **29**, 519–672 (1998).
[17] Wang, X. D., Meguid, S. A.: On the electroelastic behaviour of a thin piezoelectric actuator attached to an infinite host structure. Int. J. Solids Struct. **37**, 3231–3251 (2000).
[18] Zhang, J. Q., Zhang, B. N., Fan, J. H.: A coupled electromechanical analysis of a piezoelectric layer bonded to an elastic substrate: Part I, development of governing equations. Int. J. Solids Struct. **40**, 6781–6797 (2003).
[19] Zhang, B. N., Zhang, J. Q., Fan, J. H.: A coupled electromechanical analysis of a piezoelectric layer bonded to an elastic substrate: Part II, numerical solution and applications. Int. J. Solids Struct. **40**, 6799–6612 (2003).
[20] Gibbs, G. P., Fuller, C. R.: Excitation of thin beams using asymmetric piezoelectric actuators. J. Acoust. Soc. Am. **92**, 3221–3227 (1992).
[21] Lee, C. K., O'Sullivan, T. C.: Piezoelectric strain gages. J. Acoust. Soci. Am. **90**, 945–953 (1991).
[22] Collins, K., Plau, R., Wauer, J.: Free and forced longitudinal vibrations of cantilevered bar with a crack. ASME J. Vibr. Acoust. **114**, 171–177 (1992).
[23] Clark, R. L., Burdisso, R. A., Fuller, C. R.: Design approaches for shaping polyvinylidene fluoride sensors in active strutural acoustic control. J. Intell. Mat. Syst. Struct. **4**, 354–365 (1993).
[24] D'Cruz, J.: Active control of panel vibrations with piezoelectric actuators. J. Intell. Mat. Syst. Struct. **4**, 398–402 (1993).
[25] Choi, K. Y., Chang, F. K.: Identification of foreign object impact in structures using distributed sensors. J. Intell. Mat. Syst. Struct. **5**, 864–869 (1994).
[26] Chang, F. K.: Built-in damage diagnostics for composite structures. Proc. 10th Int. Conf. Compos. Struct. **5**, 283–289 (1995).
[27] Schulz, M. J., Pai, P. F., Inman, D. J.: Health monitoring and active control of composite structures using piezoelectric patches. Compos. Part B **30**, 713–725 (1999).
[28] Lee, C. K., Moon, F. C.: Modal sensors/actuators. ASME J. Appl. Mech. **57**, 434–441 (1990).
[29] Giurgiutiu, V., Rogers, C. A.: Modeling of the electro-mechanical (E/M) impedance response of a damaged composite beam. Adapt. Struct. Mat. Syst. **59**, 39–46 (1999).
[30] Giurgiutiu, V., Zagrai, A.: Embedded self-sensing piezoelectric active sensors for on-line structural identification. ASME J. Vibr. Acoust. **124**, 116–124 (2002).
[31] Giurgiutiu, V., Zagrai, A., Bao, J.: Embedded active sensors for in-situ structural health monitoring of thin-wall structures. ASME J. Pressure Vessel Technol. **124**, 134–145 (2002).
[32] Charette, F., Guigou, C., Bery, A., Plantier, G.: Asymmetric actuation and sensing of a beam using piezoelectric materials. J. Acoust. Soc. Am. **96**, 2272–2283 (1994).
[33] Sirohi, J., Chopra, I.: Fundamental understanding of piezoelectric strain sensors. J. Intell. Mat. Syst. Struct. **11**, 246–257 (2000).
[34] Wang, X. D., Huang, G. L.: The coupled dynamic behaviour of piezoelectric sensors bonded to elastic media. J. Intell. Mat. Syst. Struct. **17**, 884–894 (2006).
[35] Lee, C. K., Moon, F. C.: Laminated piezopolymer plates for torsion and bending sensors and actuators. J. Acoust. Soc. Am. **85**, 2432–2439 (1989).
[36] Achenbach, J. D.: Wave propagation in elastic solids. Amsterdam: North-Holland Publishing Company 1973.
[37] Pak, Y. E.: Crack extension force in a piezoelectric material. J. Appl. Mech. **57**, 647–653 (1990).